Latin American Journal of Solids and Structures
www.lajss.org

# Numerical verification and experimental validation of the FEM model of collecting electrodes in a dry electrostatic precipitator

**Abstract**

The subject of the present work is the numerical verification and experimental validation of the FEM model which would enable us to analyse the vibrations of collecting electrodes. The effectiveness of electrostatic precipitators (ESP) depends on many factors. One of these factors is the efficiency of periodic cleaning of the collecting electrodes; thus the dust is removed by inducing vibrations. These vibrations are caused by the axial impact of a hammer on an anvil beam. In the course of the impact, and afterwards, the stresses due to the impact are produced in both the rapper system and in the collecting electrode section. The paper presents a modified finite element method which can be used in simulations and to analyse the vibrations of collecting electrodes. In the verification process the calculation results obtained were compared with those from commercial software (Abaqus). The calculations and measured results were compared for validation. The comparisons were made using peak and RMS (root-mean-squared) values as well as special factors and hit rates. An acceptable compatibility of the results proves that the model can be applied in the analysis of vibrations of electrodes in design practice.

**Keywords**

Laminate Composite Plate, Finite Element, Higher Order Shear Deformation, Locking Phenomenon, Assumed Strain Method

**Andrzej Nowak**

Department of Transport and Informatics, University of Bielsko-Biala, Poland

## 1 INTRODUCTION

Electrostatic precipitation is a commonly used method for removing fine particles from airstreams. The effectiveness of these devices depends on many factors, such as the charging of particles, transporting the charged particles to the collecting surfaces, precipitation of the charged particles onto the collecting surfaces, neutralising the charged particles on the collecting surfaces, removing the particles from the collecting surface to the hopper, and conveying the particles from the hopper to a disposal point [1-4]. This research is only focused on one of these phenomena, i.e. the dislodging of particles. Removing dust collected on the electrodes is achieved by bringing them to vibrate with accelerations that allow for the effective separation of dust coagulated on their surface.

The collecting electrodes are rapped by a number of methods [5-7]. Generally, precipitator manufacturers use hammer and anvil rappers to remove particles from the collecting electrodes. One rapper system uses hammers mounted on a rotating shaft, as shown in Figure 1. As the shaft (1) rotates, the hammers (2) drop (by gravity) and strike the anvils (5) of the anvil beams (3) that are attached to the collecting electrodes (4). The weight of the hammers and the length of their mounting arm control the rapping intensity. The frequency of the rapping can be changed by adjusting the speed of the rotating shafts. Thus, rapping intensity and frequency can be adjusted for the varying dust concentration of the flue gas.

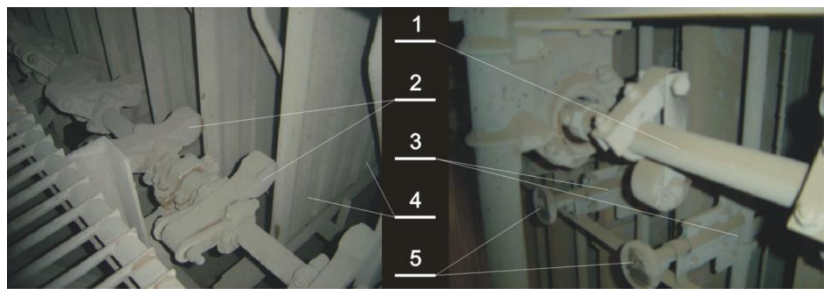


Figure 1. Rapper system.

The next chapter presents a computational model that allowed to simulate the vibrations of collecting electrodes caused when struck during the process of shaking off dust. It has been assumed that an average class PC should be sufficient to do all of the computations, and the calculation time should not exceed several dozen minutes. Two methods were used to model the arrangement: the deformable finite element method (FEM)[8] and the rigid finite element method (RFEM)[9].

Chapter 3 presents the results of verification and validation of the model. Within the verification, and besides establishing an integration step and the density of the digitised grid of electrode plates that provide adequate precision (and convergence) of the calculation results, the results of our own calculations were compared with the results received using the Abaqus commercial package. Within the process of validation, conformity of the results of our own calculations was compared with the results of measurements conducted on a special test stand.

## 2. COMPUTATIONAL MODEL

An essential feature of the finite element method is both its ability to handle complicated geometries (and boundaries) [8], [10] and its implementation in many commercial packages and open source software. Despite the existing commercial software, it is still necessary to search for more efficient solutions which are less sophisticated but more tailored to designers' specific needs. This is the case when modelling the collecting electrode system (CES) of electrostatic precipitators (Fig. 2).

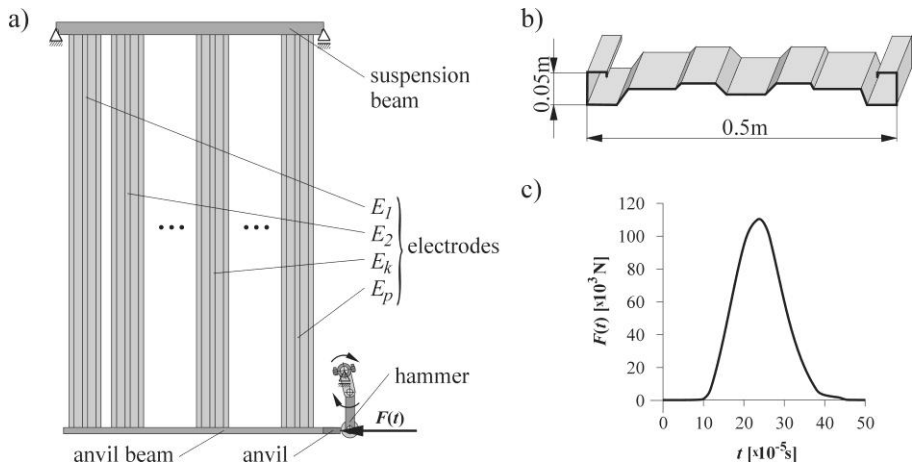


Figure 2. The most important aspects of modelling: a) schematic view of a collecting electrode system, b) SIGMA VI profile, ) measured force impulse F(t). Vibrations are generated as the system's response for a single force impulse F(t).

The model combines the finite element method (FEM) used to describe spring deformations [11] and mass and geometrical features of the collecting electrodes with the rigid finite element method (RFEM) [9], [12] used to reflect the behaviour of the beam segments of the modelled system. The remaining constructional elements, such as the joints that fasten the electrodes to the suspension beam, distance-marking bushes and riveted and screw joints, were considered in the model as concentrated masses. Equations of motion of individual sub-systems (electrodes and beams) and of the whole system were derived in the present paper from Lagrange's equations of second order. In this paper both geometrical and physical linear systems are taken into consideration (vibrations around the static equilibrium position). That is why it is possible to present the kinetic and potential energy of deformation in quadratic forms:

$$T = \frac{1}{2}\dot{\mathbf{q}}^T \mathbf{M}\dot{\mathbf{q}}\,, \tag{1}$$

$$V_s = \frac{1}{2}\mathbf{q}^{\mathrm{T}}\mathbf{C}\mathbf{q}\,, \tag{2}$$

where $\mathbf{M}$, $\mathbf{C}$ are matrices with constant elements and $\mathbf{q}$ is the vector of generalised coordinates. If the damping is passed over, then the application of Lagrange's equation leads to the following equations of the system's motion:

$$\mathbf{M}\ddot{\mathbf{q}} + \mathbf{C}\mathbf{q} = -\mathbf{G} + \mathbf{Q}\,, \tag{3}$$

where $\mathbf{M}$ is the mass matrix, $\mathbf{C}$ is the stiffness matrix, $\mathbf{G} = \dfrac{\partial V_g}{\partial \mathbf{q}}$, $V_g$ is the potential energy of gravity forces, $\mathbf{Q} = \begin{bmatrix} Q_1 & \dots & Q_n \end{bmatrix}^{\mathrm{T}}$ is the vector of generalised forces and $n$ is the number of degrees

of the system's freedom. Thus, to formulate equations of the system's (sub-system's) motion, one should determine the mass matrix $\mathbf{M}$, the stiffness matrix $\mathbf{C}$, as well as vectors $\mathbf{G}$ and Q.
The next sub-sections contain the basic relations that will allow to determine the matrices and vectors from (3) for electrodes treated as shells modelled with the deformable finite element method (FEM) [8]. A brief way will also be presented of discretising the beams modelled with the rigid finite element method (RFEM), the model of joining elements which connect the beams and electrodes, as well as the aggregation of the sub-systems' motion equations to equations for the whole system.

### 2.1 Model of shell elements

With electrode $k$ a co-ordinate system is connected with axes directed as in Fig. 3. A single electrode strip has both a constant width and thickness.

This suggests how it should be divided into elements. It is assumed that the strips are numbered from $1 \div m_k$, where the first strip on the left has the number 1 while the last strip on the right has the number $m_k$. In the $\hat{\mathbf{x}}$ direction, the strip is divided into $n_k$ elements with a length of:

$$\Delta x_k = \frac{l_k}{n_k}, \tag{5}$$

where $l_k$ is the length of the plate (and the length of the strip is $1 \div m_k$).

Thus, the whole collecting electrode is divided into:

$$n_e^{(k)} = m_k n_k, \tag{6}$$

elements.

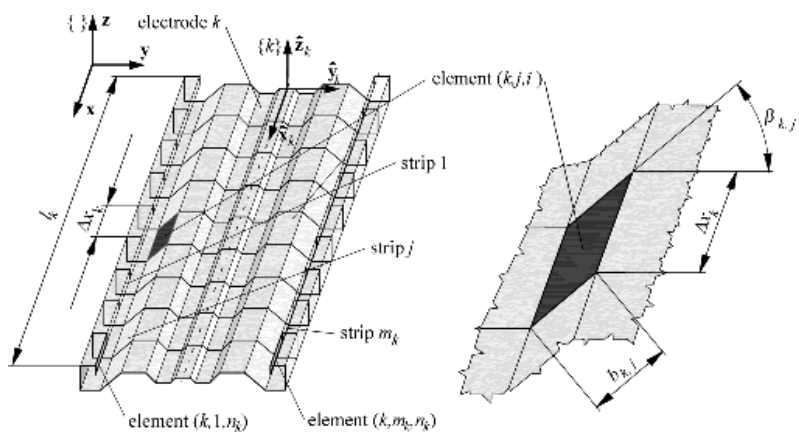


Figure 3. Strip $j$ with width $b_{k,j}$ and inclination angle $\beta_{k,j}$ towards the $\hat{\mathbf{y}}$ axis:
– system of global coordinates, $k$ – co-ordinate system connected with electrode $k$, with axes parallel to the axis of system .

The strain energy of an element with the number $k,j,i$ (Fig. 3) is independent of $i$ (in view of the division into elements with a constant length of $\Delta x_k$ in direction $\hat{\mathbf{x}}$) and from angle $\beta_{k,j}$. A rectangular four-node element, as presented in Fig. 4a, is considered here.

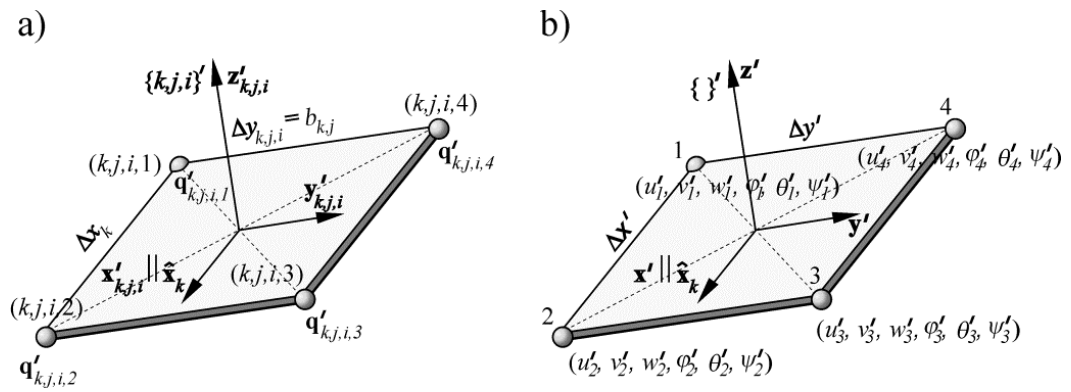


Figure 4. Four-node shell element: a) taking into consideration the following indexes: $k$ – plate, $j$ – strip, $i$ – element of strip $j$, b) passing over indexes $k$, $j$ and $i$.

The nodal displacements of the element are described by the following values:

$$\mathbf{q}'_{k,j,i,s} = \left[ u'_{k,j,i,s}, v'_{k,j,i,s}, w'_{k,j,i,s}, \varphi'_{k,j,i,s}, \theta'_{k,j,i,s}, \psi'_{k,j,i,s} \right]^{\mathrm{T}} \text{ for } s = 1,\ 2,\ 3,\ 4\,, \tag{7}$$

where $u'_{k,j,i,s}$, $v'_{k,j,i,s}$, $w'_{k,j,i,s}$ are displacements of node $k,j,i,s$ in the direction of the $\mathbf{x}'_{k,j,i}$, $\mathbf{y}'_{k,j,i}$, $\mathbf{z}'_{k,j,i}$ axes, respectively, and $\varphi'_{k,j,i,s}$, $\theta'_{k,j,i,s}$, $\psi'_{k,j,i,s}$ are rotations in the node around the axis parallel to $\mathbf{x}'_{k,j,i}, \mathbf{y}'_{k,j,i}$, $\mathbf{z}'_{k,j,i}$, respectively. In further considerations, during which the potential strain energy of the element and its kinetic energy were described, indexes *(k,j,i)* were omitted to simplify the notation. Thus, the presented procedure refers to the element from Fig. 4b.
The nodal displacements are described by the following values:

$$\mathbf{q}'_s = \left[ u'_s, v'_s, w'_s, \varphi'_s\ , \theta'_s\ , \psi'_s\ \right]^{\mathrm{T}} \text{ for } s = 1,\ 2,\ 3,\ 4\,, \tag{8}$$

It is assumed that the shield state is described by displacements $u'_s, v'_s$ and rotation angles $\psi'_s$, while displacement field $u', v'$ is described by the functions:

$$u'(x',y',t) = a_1^u + a_2^u x' + a_3^u y' + a_4^u x'y' + a_5^u (y')^2 + a_6^u x'(y')^2, \tag{9af}$$

$$v'(x',y',t) = a_1^v + a_2^v x' + a_3^v y' + a_4^v x'y' + a_5^v (x')^2 + a_6^v (x')^2 y', \tag{9b}$$

and $\psi'$ is described by relation [13]:

$$\psi' = \frac{1}{2}\left(-\frac{\partial u'}{\partial y'} + \frac{\partial v'}{\partial x'}\right). \tag{9c}$$

It is assumed that the plate state is described by deflection $w'$ and angles $\varphi'$, $\theta'$, which are described by the following relations:

$$\begin{aligned} w'\ \ x',y',t\ \ &= a_1^{(w)} + a_2^{(w)}x' + a_3^{(w)}y' + a_4^{(w)}(x')^2 + a_5^{(w)}x'y' + a_6^{(w)}(y')^2 \\ &+ a_7^{(w)}(x')^3 + a_8^{(w)}(x')^2y' + a_9^{(w)}x'(y')^2 + a_{10}^{(w)}(y')^3 \\ &+ a_{11}^{(w)}(x')^3y' + a_{12}^{(w)}x'(y')^3, \end{aligned} \tag{10a}$$

$$\varphi' = \frac{\partial w'}{\partial y'}, \tag{10b}$$

$$\theta' = -\frac{\partial w'}{\partial x'}. \tag{10c}$$

Factors $a_1^{(u)} \div a_6^{(u)}$, $a_1^{(v)} \div a_6^{(v)}$ and $a_1^{(w)} \div a_{12}^{(w)}$ can be determined from the respective boundary conditions:

$$\left.\begin{array}{lll} u'\left(-\frac{\Delta x'}{2},-\frac{\Delta y'}{2}\right) = u_1'\ \ t\ , & u'\left(\frac{\Delta x'}{2},-\frac{\Delta y'}{2}\right) = u_2'\ \ t\ , & u'\left(\frac{\Delta x'}{2},\frac{\Delta y'}{2}\right) = u_3'\ \ t\ , \\ u'\left(-\frac{\Delta x'}{2},\frac{\Delta y'}{2}\right) = u_4'\ \ t\ , & \frac{\partial u'}{\partial y'}\left(\frac{\Delta x'}{2},-\frac{\Delta y'}{2}\right) = u_{2,y}'\ \ t\ , & \frac{\partial u'}{\partial y'}\left(-\frac{\Delta x'}{2},\frac{\Delta y'}{2}\right) = u_{4,y}'\ \ t \end{array}\right\}, \tag{11a}$$

$$\left.\begin{array}{lll} v'\left(-\frac{\Delta x'}{2},-\frac{\Delta y'}{2}\right) = v_1'\ \ t\ , & v'\left(\frac{\Delta x'}{2},-\frac{\Delta y'}{2}\right) = v_2', & v'\left(\frac{\Delta x'}{2},\frac{\Delta y'}{2}\right) = v_3' \\ v'\left(-\frac{\Delta x'}{2},\frac{\Delta y'}{2}\right) = v_4', & \frac{\partial v'}{\partial x'}\left(-\frac{\Delta x'}{2},-\frac{\Delta y'}{2}\right) = v_{1,x}'\ \ t\ , & \frac{\partial v'}{\partial x'}\left(\frac{\Delta x'}{2},\frac{\Delta y'}{2}\right) = v_{3,x}'\ \ t \end{array}\right\}, \tag{11b}$$

$$w'\left(-\frac{\Delta x'}{2},-\frac{\Delta y'}{2}\right) = w_1'\ \ t\ ,\ \ \frac{\partial w'}{\partial y'}\left(-\frac{\Delta x'}{2},-\frac{\Delta y'}{2}\right) = \varphi_1'\ \ t\ ,\ \ -\frac{\partial w'}{\partial x'}\left(-\frac{\Delta x'}{2},-\frac{\Delta y'}{2}\right) = \theta_1'\ \ t\ \Big\}, \tag{11c}$$

$$w'\left(\frac{\Delta x'}{2},-\frac{\Delta y'}{2}\right) = w_2'\ \ t\ ,\ \ \frac{\partial w'}{\partial y'}\left(\frac{\Delta x'}{2},-\frac{\Delta y'}{2}\right) = \varphi_2'\ \ t\ ,\ \ -\frac{\partial w'}{\partial x'}\left(\frac{\Delta x'}{2},-\frac{\Delta y'}{2}\right) = \theta_2'\ \ t\ \Big\}, \tag{11d}$$

$$w'\left(\frac{\Delta x'}{2},\frac{\Delta y'}{2}\right) = w_3'\ \ t\ ,\ \ \frac{\partial w'}{\partial y'}\left(\frac{\Delta x'}{2},\frac{\Delta y'}{2}\right) = \varphi_3'\ \ t\ ,\ \ -\frac{\partial w'}{\partial x'}\left(\frac{\Delta x'}{2},\frac{\Delta y'}{2}\right) = \theta_3'\ \ t\ \Big\}, \tag{11e}$$

$$w'\left(-\frac{\Delta x'}{2},\frac{\Delta y'}{2}\right)=w'_4\ \ t\ ,\ \ \frac{\partial w'}{\partial y'}\left(-\frac{\Delta x'}{2},\frac{\Delta y'}{2}\right)=\varphi'_4\ \ t\ ,\ \ -\frac{\partial w'}{\partial x'}\left(-\frac{\Delta x'}{2},\frac{\Delta y'}{2}\right)=\theta'_4\ \ t\ \Big\}. \tag{11f}$$

The strain energy of the shell element in Fig. 5b is the sum of:

$$E=E^{(t)}+E^{(p)}, \tag{12}$$

where $E^{(t)}$ is the energy of the shield state and $E^{(p)}$ is the energy of the plate state. The strain energy of the element, after necessary transformations [11], can be presented in the form of:

$$\begin{aligned}E&=\tfrac{1}{2}\Big[\big[\mathbf{q}'_1\big]^{\mathrm{T}}\quad\big[\mathbf{q}'_2\big]^{\mathrm{T}}\quad\big[\mathbf{q}'_3\big]^{\mathrm{T}}\quad\big[\mathbf{q}'_4\big]^{\mathrm{T}}\Big]\begin{bmatrix}\mathbf{C}'_{1,1}&\mathbf{C}'_{1,2}&\mathbf{C}'_{1,3}&\mathbf{C}'_{1,4}\\ \mathbf{C}'_{2,1}&\mathbf{C}'_{2,2}&\mathbf{C}'_{2,3}&\mathbf{C}'_{2,4}\\ \mathbf{C}'_{3,1}&\mathbf{C}'_{3,2}&\mathbf{C}'_{3,3}&\mathbf{C}'_{3,4}\\ \mathbf{C}'_{4,1}&\mathbf{C}'_{4,2}&\mathbf{C}'_{4,3}&\mathbf{C}'_{4,4}\end{bmatrix}\begin{bmatrix}\mathbf{q}'_1\\ \mathbf{q}'_2\\ \mathbf{q}'_3\\ \mathbf{q}'_4\end{bmatrix}=\\ &=\tfrac{1}{2}\big[\mathbf{q}'\big]^{\mathrm{T}}\mathbf{C}'\mathbf{q}'=\tfrac{1}{2}\sum_{l\ 1}^{4}\sum_{s\ 1}^{4}\mathbf{q}_l'^{\mathrm{T}}\mathbf{C}'_{l,s}\mathbf{q}'_s,\end{aligned} \tag{13}$$

Where $\mathbf{q}'_s$ are specified in (8), $\mathbf{q}'=\Big[\mathbf{q}_1'^{\mathrm{T}}\quad\mathbf{q}_2'^{\mathrm{T}}\quad\mathbf{q}_3'^{\mathrm{T}}\quad\mathbf{q}_4'^{\mathrm{T}}\Big]^{\mathrm{T}}$ and $\mathbf{C}'$ is the square, symmetric stiffness matrix of an element with dimensions of $24\times24$.
It should be noted that for the defined physical parameters of plates $E,\nu,\rho,h$, the stiffness matrices of the elements depend only on dimensions $\Delta x'=\Delta x_k$ and $\Delta y'=b_{k,j}$. In view of the designation in Fig. 4 and relation (5), in the discussed case:

$$\mathbf{C}'_{k,j,i}=\mathbf{C}'_{k,j}=\mathbf{C}'\ \ \Delta x_k,b_{k,j}\ \ , \tag{14}$$

for $i=1,\ \ldots\ ,\ n_k;\quad j=1,\ \ldots\ ,\ m_k$. The formula for the strain energy of element *(k,j,i)* may be presented in the following form:

$$E_{k,j,i}=\tfrac{1}{2}\sum_{l-1}^{4}\sum_{s-1}^{4}\mathbf{q}_{k,j,i,l}'^{\mathrm{T}}\mathbf{C}'_{k,j,i,l,s}\mathbf{q}'_{k,j,i,s}\,. \tag{15}$$

Thus, as a result of adopting a constant length of $\Delta x_k$ elements, the stiffness matrix of electrode $k$ is calculated only for $j=1,\ \ldots\ ,\ m_k$, because the stiffness matrices of elements $k,j,i$ of the single strip are identical.
The kinetic energy of an element may be calculated with the following formula:

$$T = \tfrac{1}{2}\ \dot{\bar{\mathbf{u}}}^{\ \mathrm{T}}\ \bar{\mathbf{M}}^{(u)}\ \dot{\bar{\mathbf{u}}} + \tfrac{1}{2}\ \dot{\bar{\mathbf{v}}}^{\ \mathrm{T}}\ \bar{\mathbf{M}}^{(v)}\ \dot{\bar{\mathbf{v}}} + \tfrac{1}{2}\ \dot{\mathbf{q}}^{\prime(p)\ \mathrm{T}}\ \mathbf{M}^{\prime(p)}\ \dot{\mathbf{q}}^{\prime(p)}, \tag{16}$$

where $\bar{\mathbf{M}}^{(u)}, \bar{\mathbf{M}}^{(v)}$ are matrices with dimensions of 6 x 6 while $\mathbf{M}^{\prime(p)}$ is the matrix with dimensions of $12 \times 12$ with constant elements.

If the definition of vectors of nodal displacements as described in (8) is taken into consideration, then, after a proper rearrangement that runs analogically as in the case of the $\mathbf{C}'$ stiffness matrix, the expression for the kinetic energy of an element can be recorded in the following form:

$$T = \tfrac{1}{2}\dot{\mathbf{q}}'^{\mathrm{T}}\ \mathbf{M}'\dot{\mathbf{q}}' = \tfrac{1}{2}\sum_{l-1}^{4}\sum_{s-1}^{4}\dot{\mathbf{q}}_l'^{\mathrm{T}}\ \mathbf{M}'_{l,s}\dot{\mathbf{q}}'_s, \tag{17}$$

where $\mathbf{M}'_{l,s}$ are the matrices with dimensions of $6 \times 6$ with constant elements.

As is in the case of formulae for strain energy, the expression for the kinetic energy of element $k, j, i$ may be presented in the following form:

$$T_{k,j,i} = \tfrac{1}{2}\sum_{l-1}^{4}\sum_{s-1}^{4}\dot{\mathbf{q}}'^{\mathrm{T}}_{k,j,i,l}\mathbf{M}'_{k,j,i,l,s}\dot{\mathbf{q}}'_{k,j,i,s}\,. \tag{18}$$

In the computational model, the nodal displacements, expressed not in local systems but in a global co-ordinate system (5), are adopted as generalised coordinates.

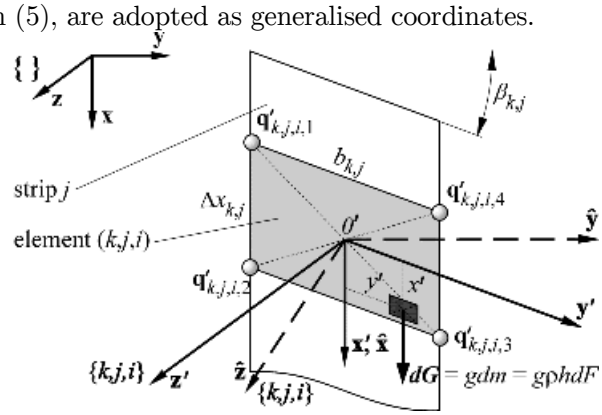


Figure 5. Element $k, j, i$ .

Let us define the following vectors:

$$\mathbf{\Delta}_{k,j,i,s} = \begin{bmatrix} u_{k,j,i,s} & v_{k,j,i,s} & w_{k,j,i,s} \end{bmatrix}^{\mathrm{T}},\ \mathbf{\Delta}'_{k,j,i,s} = \begin{bmatrix} u'_{k,j,i,s} & v'_{k,j,i,s} & w'_{k,j,i,s} \end{bmatrix}^{\mathrm{T}}, \tag{19a}$$

$$\mathbf{\Phi}_{k,j,i,s} = \begin{bmatrix} \varphi_{k,j,i,s} & \theta_{k,j,i,s} & \psi_{k,j,i,s} \end{bmatrix}^{\mathrm{T}},\ \mathbf{\Phi}'_{k,j,i,s} = \begin{bmatrix} \varphi'_{k,j,i,s} & \theta'_{k,j,i,s} & \psi'_{k,j,i,s} \end{bmatrix}^{\mathrm{T}}, \tag{19a}$$

where $\boldsymbol{\Delta}'_{k,j,i,s}$, $\boldsymbol{\Phi}'_{k,j,i,s}$ are the vectors of nodal displacements and rotations in the $k,j,i'$ system; $\boldsymbol{\Delta}_{k,j,i,s}$, $\boldsymbol{\Phi}_{k,j,i,s}$ are the vectors of nodal displacements and rotations in the $k,j,i$ system, with axes parallel to the axis of the global system and a beginning that coincides with the beginning of the $k,j,i'$ system. The following relations exist between them:

$$\boldsymbol{\Delta}_{k,j,i,s} = \bar{\mathbf{R}}_{k,j}\boldsymbol{\Delta}'_{k,j,i,s} \equiv \boldsymbol{\Delta}'_{k,j,i,s} = \bar{\mathbf{R}}^{\mathrm{T}}_{k,j}\boldsymbol{\Delta}_{k,j,i,s}\,, \tag{20a}$$

$$\boldsymbol{\Phi}_{k,j,i,s} = \bar{\mathbf{R}}_{k,j}\boldsymbol{\Phi}'_{k,j,i,s} \equiv \boldsymbol{\Phi}'_{k,j,i,s} = \bar{\mathbf{R}}^{\mathrm{T}}_{k,j}\boldsymbol{\Phi}_{k,j,i,s}\,, \tag{20b}$$

where $\bar{\mathbf{R}}_{k,j} = \begin{bmatrix} 1 & 0 & 0 \\ 0 & \cos\beta_{k,j} & -\sin\beta_{k,j} \\ 0 & \sin\beta_{k,j} & \cos\beta_{k,j} \end{bmatrix}$.

Vectors $\mathbf{q}_{k,j,i,s}$ and $\mathbf{q}'_{k,j,i,s}$, may be presented in the following forms:

$$\mathbf{q}_{k,j,i,s} = \begin{bmatrix} \boldsymbol{\Delta}^{\mathrm{T}}_{k,j,i,s} & \boldsymbol{\Phi}^{\mathrm{T}}_{k,j,i,s} \end{bmatrix}^{\mathrm{T}}, \tag{21a}$$

$$\mathbf{q}'_{k,j,i,s} = \begin{bmatrix} \boldsymbol{\Delta}'^{\mathrm{T}}_{k,j,i,s} & \boldsymbol{\Phi}'^{\mathrm{T}}_{k,j,i,s} \end{bmatrix}^{\mathrm{T}}, \tag{21b}$$

and the relations between them are described by the formulae:

$$\mathbf{q}_{k,j,i,s} = \mathbf{R}_{k,j}\mathbf{q}'_{k,j,i,s}\,, \tag{22a}$$

$$\mathbf{q}'_{k,j,i,s} = \mathbf{R}^{\mathrm{T}}_{k,j}\mathbf{q}_{k,j,i,s}\,, \tag{22b}$$

where $\mathbf{R}_{k,j} = \begin{bmatrix} \bar{\mathbf{R}}_{k,j} & 0 \\ 0 & \bar{\mathbf{R}}_{k,j} \end{bmatrix}$.

Thus, formulae (18) and (15), which describe the kinetic and strain energy of element $(k,j,i)$, may be presented in the following forms:

$$\begin{aligned} T_{k,j,i} &= \tfrac{1}{2}\sum_{l-1}^{4}\sum_{s-1}^{4}\left[\mathbf{R}^{\mathrm{T}}_{k,j}\dot{\mathbf{q}}_{k,j,i,l}\right]^{\mathrm{T}}\mathbf{M}'_{k,j,i,l,s}\left[\mathbf{R}^{\mathrm{T}}_{k,j}\dot{\mathbf{q}}_{k,j,i,s}\right] = \\ &= \tfrac{1}{2}\sum_{l-1}^{4}\sum_{s-1}^{4}\dot{\mathbf{q}}^{\mathrm{T}}_{k,j,i,l}\mathbf{M}_{k,j,i,l,s}\dot{\mathbf{q}}_{k,j,i,s} \end{aligned} \tag{23}$$

$$E_{k,j,i} = \frac{1}{2}\sum_{l-1}^{4}\sum_{s-1}^{4}\Big[\mathbf{R}_{k,j}^{\mathrm{T}}\mathbf{q}_{k,j,i,l}\Big]^{\mathrm{T}}\mathbf{C}'_{k,j,i,l,s}\mathbf{q}_{k,j,i,s} = \\ = \frac{1}{2}\sum_{l-1}^{4}\sum_{s-1}^{4}\mathbf{q}_{k,j,i,l}^{\mathrm{T}}\mathbf{C}_{k,j,i,l,s}\mathbf{q}_{k,j,i,s} \tag{24}$$

where $\mathbf{M}_{k,j,i,l,s} = \mathbf{R}_{k,j}\mathbf{M}'_{k,j,i,l,s}\mathbf{R}_{k,j}^{\mathrm{T}}$ and $\mathbf{C}_{k,j,i,l,s} = \mathbf{R}_{k,j}\mathbf{C}'_{k,j,i,l,s}\mathbf{R}_{k,j}^{\mathrm{T}}$.

There are also gravity forces that influence the electrodes in the system, and they should be taken into consideration when formulating the equations of motion. Generalised forces that come from gravity forces may be presented in the following form:

$$\mathbf{G}_{k,j,i,s} = \tilde{\mathbf{N}}_{k,j,i}^{(u)}\check{\mathbf{H}}_{k,j,u,s}, \text{ for } s = 1,2,3,4\,, \tag{25}$$

where $\tilde{\mathbf{N}}_{k,j,i}^{(u)} = \rho g h \int_{F_{k,j}} \bar{\mathbf{N}}_{k,j,i}^{(u)} dF$, $\bar{\mathbf{N}}_{k,j}^{(u)} = \mathbf{N}^{(u)}\bar{\mathbf{A}}_{k,j}^{(u)}$, $\mathbf{N}^{(u)} = \begin{bmatrix}1 & x' & y' & x'y' & (y')^2 & x'(y')^2\end{bmatrix}$, $\bar{\mathbf{A}}_{k,j}^{(u)}$ is a matrix with constant elements, $F_{k,j} = \left\langle -\frac{\Delta x_{k,j}}{2}, \frac{\Delta x_{k,j}}{2}\right\rangle \times \left\langle -\frac{b_{k,j}}{2}, \frac{b_{k,j}}{2}\right\rangle$ is the area of element $(k,j,i)$, $\Delta x_{k,j}$ and $b_{k,j}$ are described in Fig. 5, and $\check{\mathbf{H}}_{k,j,u,s}$ is a matrix with constant coefficients.

## 2.2 Model of beam elements

When modelling the upper and lower suspension beams, the classical rigid finite element method (RFEM) was applied [9]. Fig. 6 presents the general scheme of the system. The upper beam was simply supported, while the bottom beam was rigidly connected with the electrodes and loaded with point force, as in Fig. 2c.

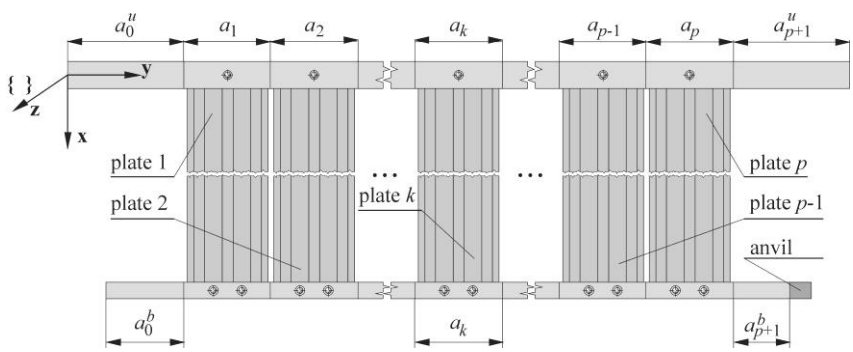


Figure 6. Geometric parameters of the electrode system.

There is a certain segment of beams $a_k$ assigned to each plate. The length of the beam segment is generally longer than the width of plate $k$. The upper and lower beams are connected to the electrodes with the help of $n_u^e$ and $n_b^e$ spring-damping elements, respectively. In practice, it is usually

assumed that $n_u^e = 1$ and $n_b^e = 2$. The way of dividing the upper and lower beams into massless and non-dimensional stiffness-damping elements *(sde)* and rigid finite elements *(rfe)* is very similar. That is why the way of dividing elements into *sde* and *rfe* is presented with a general description of the beam with the symbol $\alpha \in \{u,b\}$. Fig. 7 presents the primary and secondary division of beam $\alpha$.

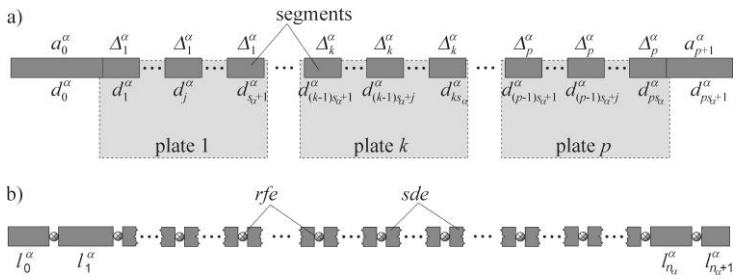


Figure 7. Division of beams into *rfe* and *sde*: a) primary, b) secondary.

It was assumed that each of the segments $a_1 \div a_p$ is divided into the same number of elements $s_\alpha$ in the primary division. Moreover, segments $a_0^\alpha$ and $a_{p+1}^\alpha$, which are usually much shorter than $a_1 \div a_p$, are not divided into smaller elements. Then, in the secondary division, the *sde* are placed in the central points of the sections. The elements lying between *sde* are treated as rigid solids (Fig. 8).

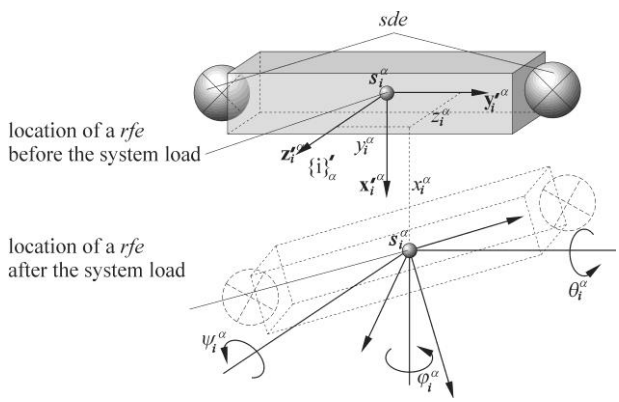


Figure 8. Generalised coordinates of *rfe i*: $x_i^a$, $y_i^a$, $z_i^a$ are translational displacements of the mass centre of *rfe i*, and $\varphi_i^\alpha$, $\theta_i^\alpha$, $\psi_i^\alpha$ are the rotational displacements of *rfe i*.

The mass parameters and coordinates of the mass centres, and thereby coordinates of *sde*, change when additional bodies (reinforcements, cross-bars, bushes, anvil, etc.) are added to the *rfe* of the upper or lower beams. In a computer implementation of the models presented here, it was assumed that the added bodies may be represented by concentrated masses. An equation of motion for the free beam may be presented in the following form:

$$\mathbf{M}^\alpha \ddot{\mathbf{q}}^\alpha + \mathbf{C}^\alpha \mathbf{q}^\alpha = -\mathbf{G}^\alpha + \mathbf{Q}^\alpha \tag{26}$$

where $\mathbf{q}^{\alpha} = \left[ \mathbf{q}_1^{\alpha\,\mathrm{T}} \ldots \mathbf{q}_i^{\alpha\,\mathrm{T}} \ldots \mathbf{q}_{n_z}^{\alpha\,\mathrm{T}} \right]^{\mathrm{T}}$ and $\mathbf{q}_i^{\alpha} = \left[ x_i^{\alpha} \quad y_i^{\alpha} \quad z_i^{\alpha} \quad \varphi_i^{\alpha} \quad \theta_i^{\alpha} \quad \psi_i^{\alpha} \right]^{\mathrm{T}}$ is a vector of the generalised coordinates *rfe i*, as in Fig. 8, $\mathbf{M}^{\alpha}$ are the diagonal mass matrices with constant coefficients, $\mathbf{C}^{\alpha}$ are the stiffness matrices with constant coefficients, $\mathbf{G}^{\alpha}$ is the vector of gravity forces and $\mathbf{Q}^{\alpha}$ is the vector of external generalised forces. It is worth mentioning that the mass matrices $\mathbf{M}^{\alpha}$ of the beams are diagonal and the stiffness matrices $\mathbf{C}^{\alpha}$ are rare matrices.

Aggregation of equations

The equations of motion of the upper and lower beams and of the electrodes, treated as free (before connecting them in a system with the help of *sde*), may be presented in the following form:

$$\mathbf{M}^{(u)}\ddot{\mathbf{q}}^{(u)} + \mathbf{C}^{(u)}\mathbf{q}^{(u)} = -\mathbf{G}^{(u)}, \tag{27}$$

$$\mathbf{M}^{(k)}\ddot{\mathbf{q}}^{(k)} + \mathbf{C}^{(k)}\mathbf{q}^{(k)} = -\mathbf{G}^{(k)} \text{ for } \quad k = 1,\ldots,p, \tag{28}$$

$$\mathbf{M}^{(b)}\ddot{\mathbf{q}}^{(b)} + \mathbf{C}^{(b)}\mathbf{q}^{(b)} = -\mathbf{G}^{(b)} + \mathbf{Q}^{(b)} \quad \mathbf{F} \quad , \tag{29}$$

where $\mathbf{M}^{(u)}$ and $\mathbf{M}^{(b)}$ are the mass matrices of the upper and lower beam (diagonal), $\mathbf{C}^{(u)}$ and $\mathbf{C}^{(b)}$ are the stiffness matrices of the upper and lower beam (rare, symmetric, with 18 non-zeroing elements at the most in each column, $\mathbf{G}^{(u)}$ and $\mathbf{G}^{(b)}$ are the gravity force vectors of the upper and lower beam, $\mathbf{Q}^{(b)}$ $\mathbf{F}$ is the vector of generalised forces induced by the action of a striking force of the beater hitting the anvil of the lower beam, with 6 non-zeroing elements at the most, $\mathbf{M}^{(k)}$ and $\mathbf{C}^{(k)}$ are the mass and stiffness matrices of the $k^{\mathrm{th}}$ electrode (rare, symmetric with 54 non-zeroing elements at the most in each column), $\mathbf{G}^{(k)}$ is the vector of gravity forces of electrode $k$, $\mathbf{q}^{(u)} = \left[ \mathbf{q}_0^{u\mathrm{T}} \quad \cdots \quad \mathbf{q}_{n^u}^{u\,\mathrm{T}} \right]^{\mathrm{T}}$, $\mathbf{q}_i^{(u)} = \left[ x_i^u \quad y_i^u \quad z_i^u \quad \varphi_i^u \quad \theta_i^u \quad \psi_i^u \right]^{\mathrm{T}}$, $\mathbf{q}^{(k)} = \left[ \mathbf{q}_{k,1}^{\mathrm{T}} \quad \cdots \quad \mathbf{q}_{k,n_w^{(k)}}^{\mathrm{T}} \right]^{\mathrm{T}}$, $\mathbf{q}_{k,i} = \left[ x_{k,i} \quad y_{k,i} \quad z_{k,i} \quad \varphi_{k,i} \quad \theta_{k,i} \quad \psi_{k,i} \right]^{\mathrm{T}}$, $\mathbf{q}^{(b)} = \left[ \mathbf{q}_0^{b\mathrm{T}} \quad \cdots \quad \mathbf{q}_{n^b}^{b\,\mathrm{T}} \right]^{\mathrm{T}}$, and $\mathbf{q}_i^{(b)} = \left[ x_i^b \quad y_i^b \quad z_i^b \quad \varphi_i^b \quad \theta_i^b \quad \psi_i^b \right]^{\mathrm{T}}$.

The introduction of flexible connections of electrodes with beams results in feedbacks between vectors $\mathbf{q}^{(u)}$ and $\mathbf{q}^{(k)}$ as well as between vectors $\mathbf{q}^{(k)}$ and $\mathbf{q}^{(b)}$.

In the present paper it was assumed that the connection of electrodes and beams is made with the help of *sde*. Fig. 9 presents the connection of the electrode element with number $k, j, i$ with *rfe* $e$ of beam $\alpha$. In structural solutions known to the author, there are always connections of beams and electrodes used in which the axes are parallel to the axis of global system $\{\ \}$ and, thereby, parallel to the axis of systems $i'_{\alpha}$ and $k, j, i' = k, j, i$. Such a solution eliminates

the need to take the rotation matrix into consideration in any further discussion. The vector of strain of *sde h* may be described with the formula:

$$\mathbf{\Delta}_h = \mathbf{A}_h^{ses}\mathbf{q}_e^{\alpha} - \sum_{s-1}^{4}\mathbf{A}_h^{mes}\mathbf{q}_{k,j,i,s}\,, \tag{30}$$

where $\mathbf{A}_h^{ses}$, $\mathbf{A}_h^{mes}$ are matrices of $6\times 6$ with constant coefficients. The strain energy may be described as:

$$V_h = \frac{1}{2}\mathbf{\Delta}_h^{\mathrm{T}}\mathbf{C}_h\mathbf{\Delta}_h\,, \tag{31}$$

where $\mathbf{C}_h = diag\ \ c_h^x \quad c_h^y \quad c_h^z \quad c_h^{\psi} \quad c_h^{\theta} \quad c_h^{\varphi}$ is the matrix of the coefficient of connection stiffness.

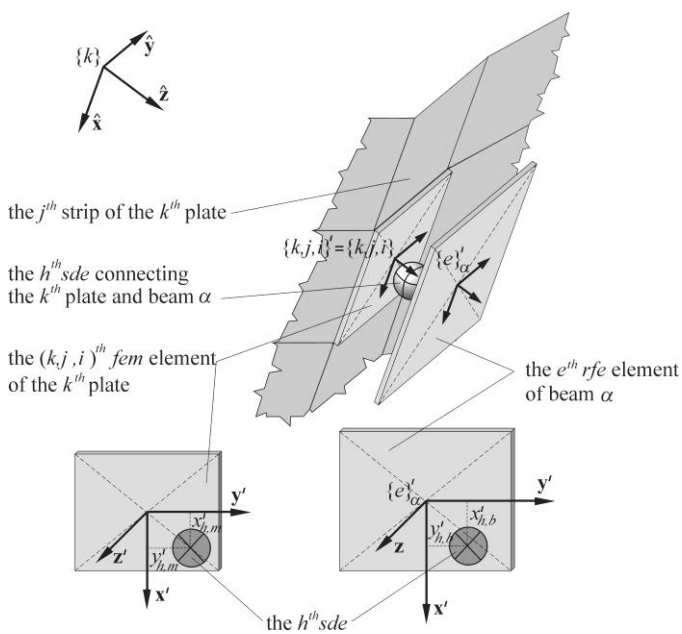


Figure 9. Stiffness-damping connection $h$ of element $k,j,i$ of plate $k$ with *rfe* $e$ of beam $\alpha$.

Differentiating (31) with regard to the generalised coordinates $\mathbf{q}_e^{\alpha}$ and $\mathbf{q}_{k,j,i,s}$, one may determine the additional elements (matrices 6 x 6) that may be added to the stiffness matrix of electrode $k$ and beam $a$. Having taken the connections into account, the equations of the system's motion take the following form:

$$\underbrace{\begin{bmatrix} \mathbf{M}^{(u)} & 0 & \cdots & 0 & \cdots & 0 & 0 \\ 0 & \mathbf{M}^{(1)} & \cdots & 0 & \cdots & 0 & 0 \\ \vdots & \vdots & \ddots & \vdots & \vdots & \vdots & \vdots \\ 0 & 0 & \cdots & \mathbf{M}^{(k)} & \cdots & 0 & 0 \\ \vdots & \vdots & \vdots & \vdots & \ddots & \vdots & \vdots \\ 0 & 0 & \cdots & 0 & \cdots & \mathbf{M}^{(p)} & 0 \\ 0 & 0 & \cdots & 0 & \cdots & 0 & \mathbf{M}^{(b)} \end{bmatrix}}_{\mathbf{M}} \underbrace{\begin{bmatrix} \ddot{\mathbf{q}}^{(u)} \\ \ddot{\mathbf{q}}^{(1)} \\ \vdots \\ \ddot{\mathbf{q}}^{(k)} \\ \vdots \\ \ddot{\mathbf{q}}^{(p)} \\ \ddot{\mathbf{q}}^{(b)} \end{bmatrix}}_{\ddot{\mathbf{q}}} +$$

$$+ \underbrace{\begin{bmatrix} \mathbf{C}^{(u)} & \mathbf{C}_1^{(u)} & \cdots & \mathbf{C}_k^{(u)} & \cdots & \mathbf{C}_p^{(u)} & 0 \\ \mathbf{C}_u^{(1)} & \mathbf{C}^{(1)} & \cdots & 0 & \cdots & 0 & \mathbf{C}_b^{(1)} \\ \vdots & \vdots & \ddots & \vdots & \vdots & \vdots & \vdots \\ \mathbf{C}_u^{(k)} & 0 & \cdots & \mathbf{C}^{(k)} & \cdots & 0 & \mathbf{C}_b^{(k)} \\ \vdots & \vdots & \vdots & \vdots & \ddots & \vdots & \vdots \\ \mathbf{C}_u^{(p)} & 0 & \cdots & 0 & \cdots & \mathbf{C}^{(p)} & \mathbf{C}_b^{(p)} \\ 0 & \mathbf{C}_1^{(b)} & \cdots & \mathbf{C}_k^{(b)} & \cdots & \mathbf{C}_p^{(b)} & \mathbf{C}^{(b)} \end{bmatrix}}_{\mathbf{C}} \underbrace{\begin{bmatrix} \mathbf{q}^{(u)} \\ \mathbf{q}^{(1)} \\ \vdots \\ \mathbf{q}^{(k)} \\ \vdots \\ \mathbf{q}^{(p)} \\ \mathbf{q}^{(b)} \end{bmatrix}}_{\mathbf{q}} = \underbrace{\begin{bmatrix} -\mathbf{G}^{(u)} \\ -\mathbf{G}^{(1)} \\ \vdots \\ -\mathbf{G}^{(k)} \\ \vdots \\ -\mathbf{G}^{(p)} \\ -\mathbf{G}^{(b)} + \mathbf{Q}^{(b)} \end{bmatrix}}_{\mathbf{f}}, \tag{32}$$

or in general form:

$$\mathbf{M}\ddot{\mathbf{q}} + \mathbf{C}\mathbf{q} = \mathbf{f}\,. \tag{33}$$

The equations of motion (33) were integrated with the Newmark method with a constant integration step.

## 3 MODEL VERIFICATION AND VALIDATION

The FEM model presented in the previous chapter was implemented into VibroESPan calculation software. The verification presented in sub-chapter 3.1 is an indirect verification that consists of performing a simulation in the VibroESPan software and of comparing the results with those received when using the Abaqus commercial package. Validation is performed by comparing the results of numerical simulations (achieved with the help of VibroESPan software) with the results of measurements on the test stand. The process of model validation is described in sub-chapter 3.2. Both during verification and validation, the system is loaded by gravitational force and the force impulse $F(t)$ applied to the anvil.

Peak value $W_{Max}$ and root-mean-square value $W_{RMS}$ were used to evaluate signals in the domain of amplitudes. These values are expressed with the following relationships:

$$W_{Max,s,\tilde{s},i} = \max_{0 \le t \le t_a} \left| a_{s,\tilde{s},i} \right|, \tag{34a}$$

$$W_{RMS,s,\ddot{s},i} = \frac{1}{t_a}\left[\int_0^{t_a} a_{s,\ddot{s},i}^2 dt\right]^{\frac{1}{2}}, \tag{34b}$$

where $t_a$ is the time of analysis, $\ddot{s}$ is the index that takes the value $\ddot{n}$ if signal $a_{s,\ddot{s},i}$ was determined as the result of numerical calculations in the FEM model, or $\ddot{p}$ if it was received in the ABQ model (in the verification process), or if it was received as the result of measurements (in the validation process), and $i$ is the number of checkpoints. In the above formulae it was assumed that $a_{s,\ddot{s},i}$ may be one of the following values:

$$a_{s,\ddot{s},i} = \begin{cases} a_{x,\ddot{s},i} & \text{- acceleration in the direction of axis } \mathbf{x}, \\ a_{y,\ddot{s},i} & \text{- acceleration in the direction of axis } \mathbf{y}, \\ a_{\tau,\ddot{s},i} = \sqrt{a_{x,\ddot{s},i}^2 + a_{y,\ddot{s},i}^2} & \text{- tangential acceleration in plane } \mathbf{xy}, \\ a_{\nu,\ddot{s},i} = a_{z,\ddot{s},i} & \text{- normal acceleration to plane } \mathbf{xy}, \\ a_{c,\ddot{s},i} = \sqrt{a_{x,\ddot{s},i}^2 + a_{y,\ddot{s},i}^2 + a_{z,\ddot{s},i}^2} & \text{- total acceleration}, \end{cases}$$

which means that $s \in \{x, y, \tau, \nu, c\}$.

The verifiability indicators *FAC2* were used as the error measure both in the process of verification and in the process of validation:

$$FAC2_{\ddot{\gamma}} = \frac{1}{n_p}\sum_{i-1}^{n_p} N_i^f \tag{35a}$$

$$N_i^f = \begin{cases} 1 & \text{for } \frac{1}{2} \le \dfrac{W_{\ddot{\gamma},s_i,\ddot{n}} \quad a_{s_i,\ddot{n}}}{W_{\ddot{\gamma},s_i,\ddot{p}} \quad a_{s_i,\ddot{p}}} < 2 \\ 0 & \text{otherwise} \end{cases} \tag{35b}$$

where $W_{\ddot{\gamma},s_i,\ddot{s}}$ and $W_{\ddot{\gamma},s_i,\ddot{s}}$ are calculated in accordance with (34), $\ddot{\gamma} \in \{Max, RMS\}$, and $n_p$ is the number of checkpoints. The hit rate $q(a_s)$ is defined as:

$$q_{\ddot{\gamma}} = \frac{1}{n_p}\sum_{i-1}^{n_p} N_i^q \tag{36a}$$

$$N_i^q = \begin{cases} 1 & \text{for } \dfrac{\left|W_{\gamma,s_i,\hat{n}} \;\; a_{s_i,\hat{n}} - W_{\gamma,s_i,\hat{p}} \;\; a_{s_i,\hat{p}}\right|}{W_{\gamma,s_i,\hat{p}} \;\; a_{s_i,\hat{p}}} < \varepsilon \;\text{ or }\; \dfrac{\left|W_{\gamma,s_i,\hat{n}} \;\; a_{s_i,\hat{n}} - W_{\gamma,s_i,\hat{p}} \;\; a_{s_i,\hat{p}}\right|}{W_{\gamma,s_i,\hat{n}} \;\; a_{s_i,\hat{n}}} < \varepsilon \\ 0 & \text{otherwise} \end{cases} \tag{36b}$$

where $\varepsilon$ is the allowable error.

### 3.1 Computational verification

The FEM model presented in Fig. 10 was applied during the remaining stages of verification and validation. The configuration of checkpoints presented in Fig. 10 corresponds to the arrangement of acceleration sensors on the test stand. Verification of the model with indicators *FAC2* and $q$ is executed for $n_p = 28$ checkpoints and $\varepsilon = 0.4$.

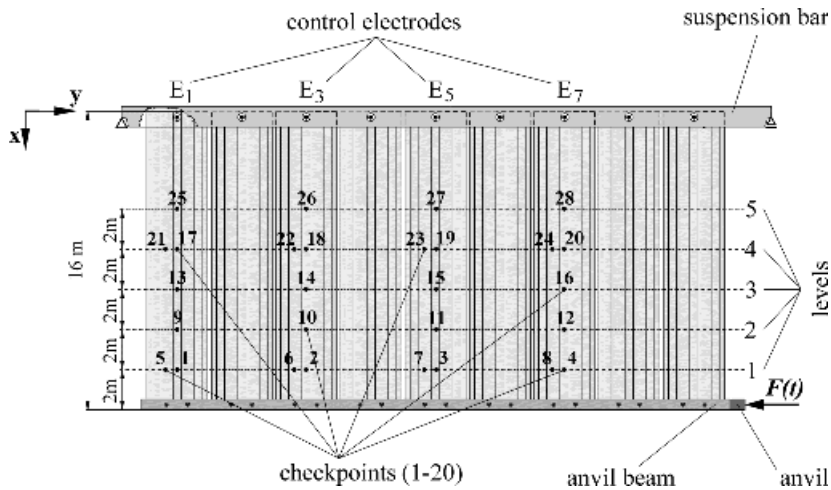


Figure 10. Model scheme with an electrode system used in verification and validation.

The values of the model's indicators calculated with reference to the results obtained from the Abaqus commercial software (ABQ model) are presented in Fig. 11. The difference in results of simulations between the FEM model and the ABQ model fluctuated between 3% and 23%, depending on the analysed acceleration (normal $a_{\nu}$, tangential $a_{\tau}$ and total $a_c$) and the indicator.

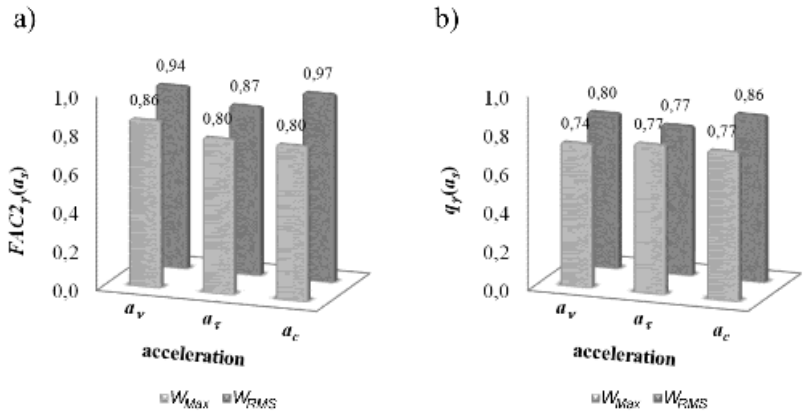


Figure 11. Verification: indicators $FAC2_{\gamma}\ a_s$ and $q_{\gamma}\ a_s$ .

The comparative analysis of amplitudes presents good conformity of both models in the scope of the $W_{RMS}$ values of accelerations, especially the values of total acceleration $a_c$. In the latter case, in 86% of the checkpoints, the values of $W_{RMS}$ are within the acceptable range of hit rate $q_{RMS}\ a_c$ and as much as 97% within the permissible range of the value of the $FAC2_{RMS}\ a_c$ indicator.

### 3.2 Measuring Validation

Verification carried out as described above allowed for an exclusion of errors in the implementation of algorithms applied in the presented model. However, a model verified with a positive result does not necessarily have to be a model that correctly describes a real object. That is why the second stage of the model's evaluation should be performed. This consists in validation that describes the correctness of the model with reference to the results of the measurements. Validation is carried out by comparing the results of numerical simulations with the results of measurements achieved on the test-bench. Conformity of the model with the object is performed by analysing the $W_{Max}\ a_{s,\dot{s}}$ and $W_{RMS}\ a_{s,\dot{s}}$ values and taking the index $FAC2_{\gamma}\ a_s$ and hit rate $q_{\gamma}\ a_s$ as error measures. Fig. 12 presents a combination of the values of $FAC2_{\gamma}\ a_s$ and $q_{\gamma}\ a_s$ .

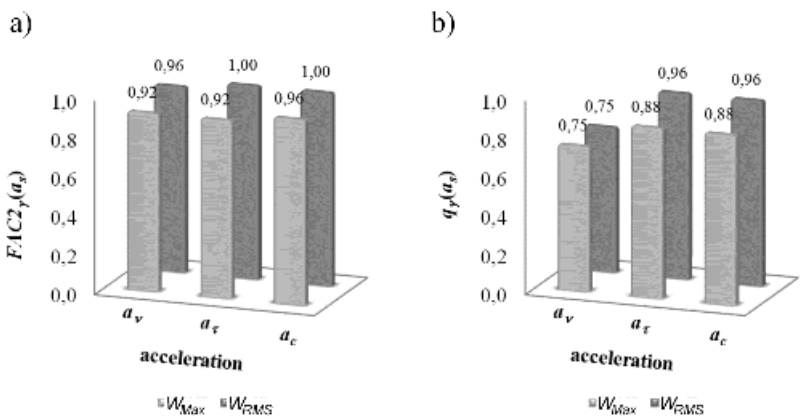

Figure 12. Validation: indexes $FAC2_{\ddot{y}}\ a_s$ and $q_{\ddot{y}}\ a_s$ .

High values of verifiability index $FAC2$ are obtained. For $FAC2_{Max}\ a_{\ddot{r}}$ , only 2 checkpoints are not within the acceptable range, whereas in the case of index $FAC2_{RMS}\ a_c$ – only one checkpoint was outside the range. The values of index $q_{\ddot{y}}\ a_s$ look slightly worse – in this case the differences in the values fluctuate between 4% and 25% (1 to 7 points). Such differences may result from the fact that the acceleration measurements themselves are burdened with errors that result indirectly or directly from the accuracy of the sensors, linearity and distortions generated by the recorder in the output signal, from the precision of positioning the sensors in the test stand, accuracy of signal synchronisation in the measurement sequences and accuracy of measurements of the force impulse. In addition, simplifications in the modelling of electrodes can be the reasons for the differences in calculations and measurement results.

## 4 CONCLUSIONS

The procedure applied in the present paper, in which sub-systems (beams and electrodes) are connected not with the help of equations of constraints, but through stiffness-damping elements, has its advantages and disadvantages. An advantage is the fact that there is no need to define additional unknowns (Lagrange's coefficients – constraint reactions). Its disadvantage is the lack of a general method of selecting the translation and rotational stiffness coefficients, *sde*, that join the subsystems.

The results of verification and validation of the model allow to state that the model correctly reflects the dynamic phenomena that appear in the system of collecting electrodes during the vibrations generated in them by an impulse of the force coming from the hammer of the rapping system. This verification and validation demonstrates some differences between the model and measurement results, but they are within the range of values accepted in engineering practice. Moreover, the results are characterised by precision comparable to the precision achieved in commercial models, yet reached at considerably smaller computational costs [11]. Computer implementation of the model, as presented in the paper, has found application in the design office of one of Poland's producers of electrostatic precipitators.

The overall conclusion is that the process of vibration excitation and wave propagation in the system of electrodes is the result of many factors [14]. This process depends not only on the impact force, but also on the physical parameters, geometry and construction of all the elements that make up this system [10]. In this respect the model presented in this paper is an important novelty, since using the testing calculations can help predict the properties of a future structure as early as in its design stage.

The author is aware of the imperfections in the presented models and results. It is the author's opinion that future research should take into consideration:

– formulation of a model element in the FEM which would better reproduce rotational stiffness, e.g. through the application of elements with a larger number of nodes,

– developing a method of choosing the coefficients of stiffness of the collecting electrode connections and beams, or replacing them with constraint equations,
– applying the wave equations for the analysis of phenomena occurring in the system of the collecting electrodes.

## Acknowledgements

This paper is an extended version of a speech delivered at the $11^{th}$ *Conference on Dynamical Systems – Theory and Applications*, 5–8 December, 2011, in Łódź, Poland.

## References

[1] Y. Yamamoto. Effects of Turbulence and Electrohydrodynamics on the Performance of Electrostatic Precipitators. *Journal of Electrostatics*, 22:11-22, 1989.
[2] Z. Long, Q. Yao, Q. Song, and S. Li. A second-order accurate finite volume method for the computation of electrical conditions inside a wire-plate electrostatic precipitator on unstructured meshes. *Journal of Electrostatics*. 67(4):597-604, 2009.
[3] S.L. Francis, A. Bäck, and P. Johansson. Reduction of Rapping Losses to Improve ESP Performance. *Proceedings ICESP XI*, Hangzhou, China; 2008.
[4] M. Sarna. Self exploring ESP rapping optimisation system. *Proceedings ICESP VI*, Budapest, Hungary, 1996.
[5] A. Nowak, and S. Wojciech. Optimisation and experimental verification of a dust-removal beater for the electrodes of electrostatic precipitators. *Computers and Structures*, 82(22):1785-1792, 2004.
[6] S.H. Kim, and K.W. Lee. Experimental study of electrostatic precipitator performance and comparison with existing theoretical prediction models. *Journal of Electrostatics*, 48:3-25, 1999.
[7] L. Buhl, S. Drue, and L. Lind. Field testing of acoustical cleaning of electrostatic precipitators. *Proceedings ICESP VI*, Budapest, Hungary, 1996.
[8] O.C. Zienkiewicz, R.L. Taylor, and J.Z. Zhu. *The finite element method: its basis and fundamentals*. $6^{th}$ ed., reprint, - Amsterdam : Elsevier Butterworth Heinemann, 2006.
[9] E. Wittbrodt, I. Adamiec-Wójcik, and S. Wojciech. *Dynamics of flexible multibody systems. Rigid finite element method*. Springer-Verlag Berlin Heidelberg, 2006.
[10] G. Rakowski, and Z. Kacprzyk. *Metoda Elementów Skończonych w mechanice konstrukcji (Finite Element Method in mechanics of structures)*. Oficyna Wydawnicza PW, Warszawa, 2005 (in Polish).
[11] I. Adamiec-Wójcik, A. Nowak, and S. Wojciech. Comparison of methods for vibration analysis of electrostatic precipitators. *Acta Mechanica Sinica*, 27(1):72-79, 2011.
[12] J. Kruszewski et al. *Metoda sztywnych elementów skończonych w dynamice konstrukcji (Finite Element Method in dynamisc of structures)*. WN-T, Warszawa, 1999 (in Polish).
[13] M. Huang, Z. Zhao, and C. Shen. An effective planar triangular element with drilling rotation. *Finite Elements in Analysis and Design*, 46: 1031-1036, 2010.
[14] A. Strchlow, M. Schmoch. Comparison of the techniques for electrode rapping in electrostatic precipitators, *Proceedings ICESP VIII*, Birmingham, AL., USA, 2001.